Autowaves and Spatio-Temporal Chaos in CNNs—Part II: A Tutorial

Ladislav Pivka

Abstract—**In this paper, we reproduce and discuss some of the spatio-temporal phenomena, recently simulated in discrete CNNs of dimension one, two, and three. We show how target, or concentric waves, can be generated in both excitable and fluctuating 2-D media, and how several types of scroll waves can be simulated in 3-D arrays. The basic property of autowaves exhibited in interactions—mutual annihilation—is demonstrated through examples. Also included is a discussion of the coexistence of low- and high-dimensional attractors in a CNN ring. Chua's circuit is used as the basic cell in the CNN arrays. Parameter values and initial conditions for the corresponding simulations are given so they can be reproduced with different simulators.**

I. Introduction

TRAVELING waves and spiral waves have been discussed in Part I of this tutorial. The same types of CNN media (excitable or fluctuating) can also be used to generate other types of wave phenomena, e.g., trigger waves and target (concentric) waves. These will be demonstrated in Section II, where we also discuss three different combinations of interaction between spiral and concentric waves in excitable media.

Three-dimensional vortex rings were first observed and described in [1]. Because of the complexity and high computational costs, three-dimensional analogs of planar spiral waves have begun to be studied in depth only recently, largely inspired by experimental observations of wave propagation in nerve and heart tissues [3], [4]. In most cases, the FitzHugh–Nagumo equations and the Oregonator model were used previously to model the dynamics in excitable media [5], [6]. Simulations of 3-D scroll waves in arrays of Chua's circuits [2] are described in Section III. Finally, in Section IV, a CNN medium is considered, in which two limit cycles are exhibited by each uncoupled neuron. Media of this type have been shown to give rise to complex spatio-temporal chaotic phenomena.

Manuscript received January 10, 1995; revised May 15, 1995. This work was supported in part by the Office of Naval Research under Grant N00014-89-J-1402 and the National Science Foundation under Grant MIP 86-14000. This paper was recommended by Guest Editor L. O. Chua.

The author is with the Electronics Research Laboratory and Department of Electrical Engineering and Computer Sciences, University of California, Berkeley, CA 94720 USA.

IEEE Log Number 9414460.

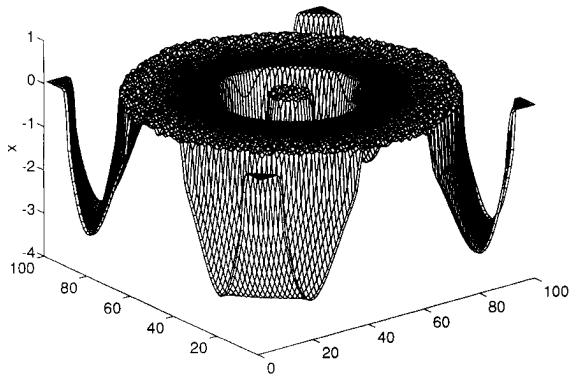

(a)

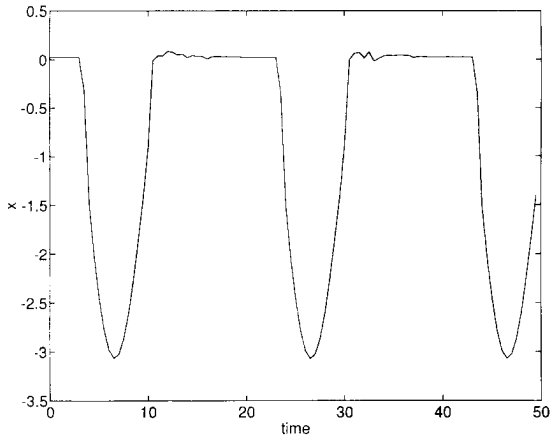

(b)

Fig. 1. (a) Target wave in a 98 × 98 array of excitable Chua's circuits, with diffusion coefficient $D = 0.5$. The variable x of cell (50, 50) was set to -3 periodically every 10 time units. (b) Time waveform of the x variable of cell (45, 45).

II. Target Waves in Excitable and Fluctuating Media

A. Target Waves in Excitable Media

We will use a 2-D excitable medium described by the following system of coupled Chua's equations

$$\begin{aligned}\dot{x}_{i,j} &= \alpha(y_{i,j} - f(x_{i,j})) \\ &\quad + D(x_{i+1,j} + x_{i-1,j} + x_{i,j+1} + x_{i,j-1} - 4x_{i,j}) \\ \dot{y}_{i,j} &= x_{i,j} - y_{i,j} + z_{i,j} \qquad (i,j = 1,2\cdots,l) \\ \dot{z}_{i,j} &= -\beta y_{i,j} \end{aligned} \tag{1}$$

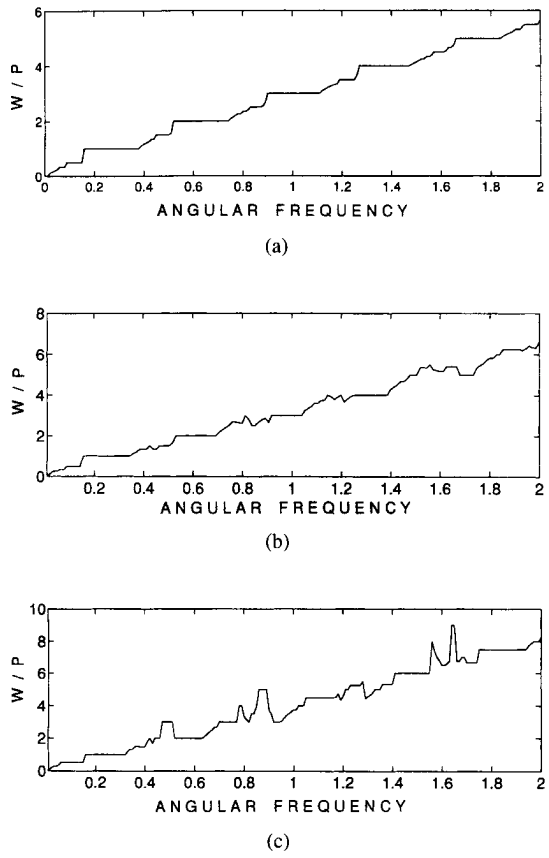

Fig. 2. Devil's staircase breakdown for decreasing coupling strength D in a 5×5 array of excitable cells. Parameter values (3) were used with $s_2 = 55.78573$ and constant amplitude of forcing $A = 1.2$. The symbol W denotes the winding number, i.e., the ratio f_s/f_d where f_s is the frequency of forcing and f_d is the system's response frequency. P denotes the period number, i.e., the number of local minima, per least period, in the waveform of one of the state variables. The cell (3, 3) was forced and the response of cell (5, 5) was monitored. (a) Devil's staircase at $D = 0.3$. (b) Devil's staircase at $D = 0.1$. (c) Devil's staircase at $D = 0.03$.

where

$$f(x) = (1/2)[(s_1 + s_2)x + (s_0 - s_1)(|x - B_1| - |B_1|) + (s_2 - s_0)(|x - B_2| - |B_2|)] + \epsilon \quad (2)$$

is a three-segment piecewise-linear function with breakpoints $B_1 = -1$ and $B_2 = 0.023744$, α and β are appropriately scaled circuit parameters, $D = \alpha/(GR)$ is the diffusion coefficient, and l is the array size.

The parameters will be chosen as follows:

$$\alpha = 10, \quad \beta = 0.3014987, \quad s_1 = 0.078573, \quad s_2 = 55, \quad s_0 = -1.25719, \quad \epsilon = 0. \quad (3)$$

In all simulations we use zero flux (Neumann) boundary conditions. With the above parameter values, each individual cell exhibits two stable equilibrium points $\mathbf{P}^+ = (-1.238, 0, 1.238)$, $\mathbf{P}^- = (0.02385, 0, -0.02385)$. When all cells are set to the stable equilibrium point $\mathbf{P}^+$, no motion can be observed, even if the diffusion coefficient D is nonzero. By perturbing one of the cells of the array a traveling wave

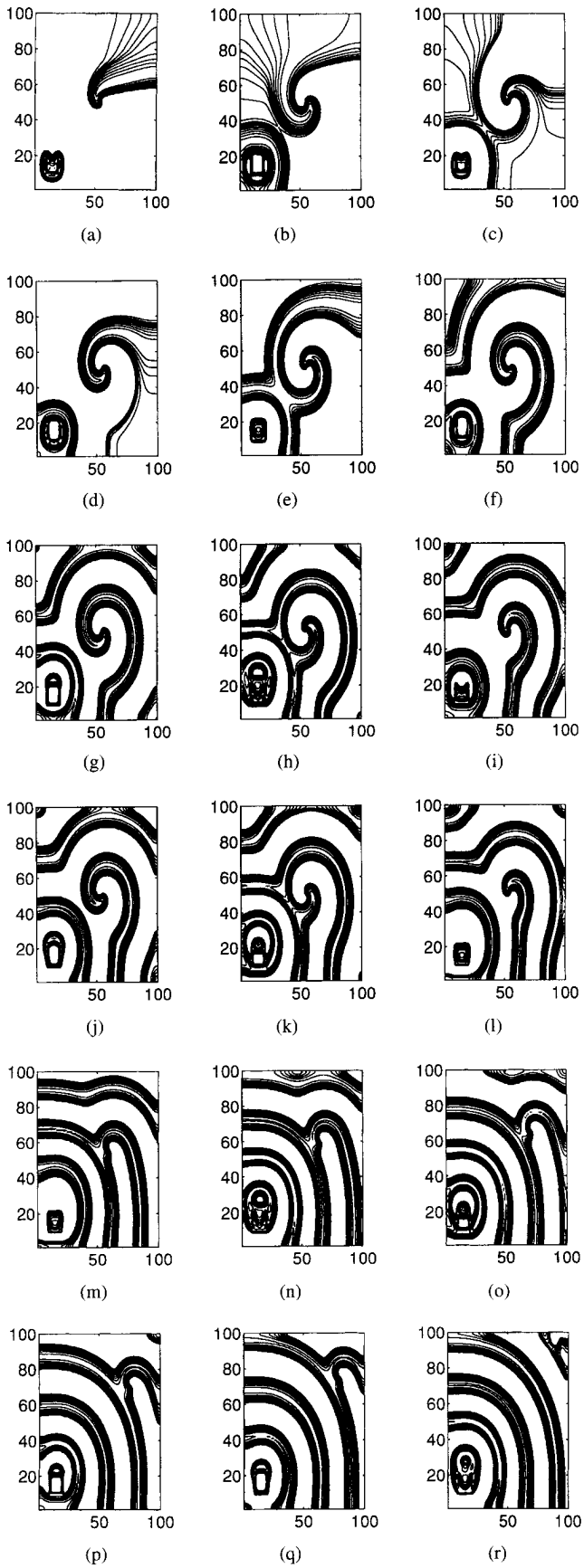

Fig. 3. Contour snapshots of target wave development in a fluctuating medium ($D = 5$) of 98×98 cells. (a) through (r) correspond to time $t =$ 20, 40, 60, 80, 100, 120, 300, 400, 500, 600, 700, 1500, 1800, 2100, 2400, 2700, and 3900, respectively.

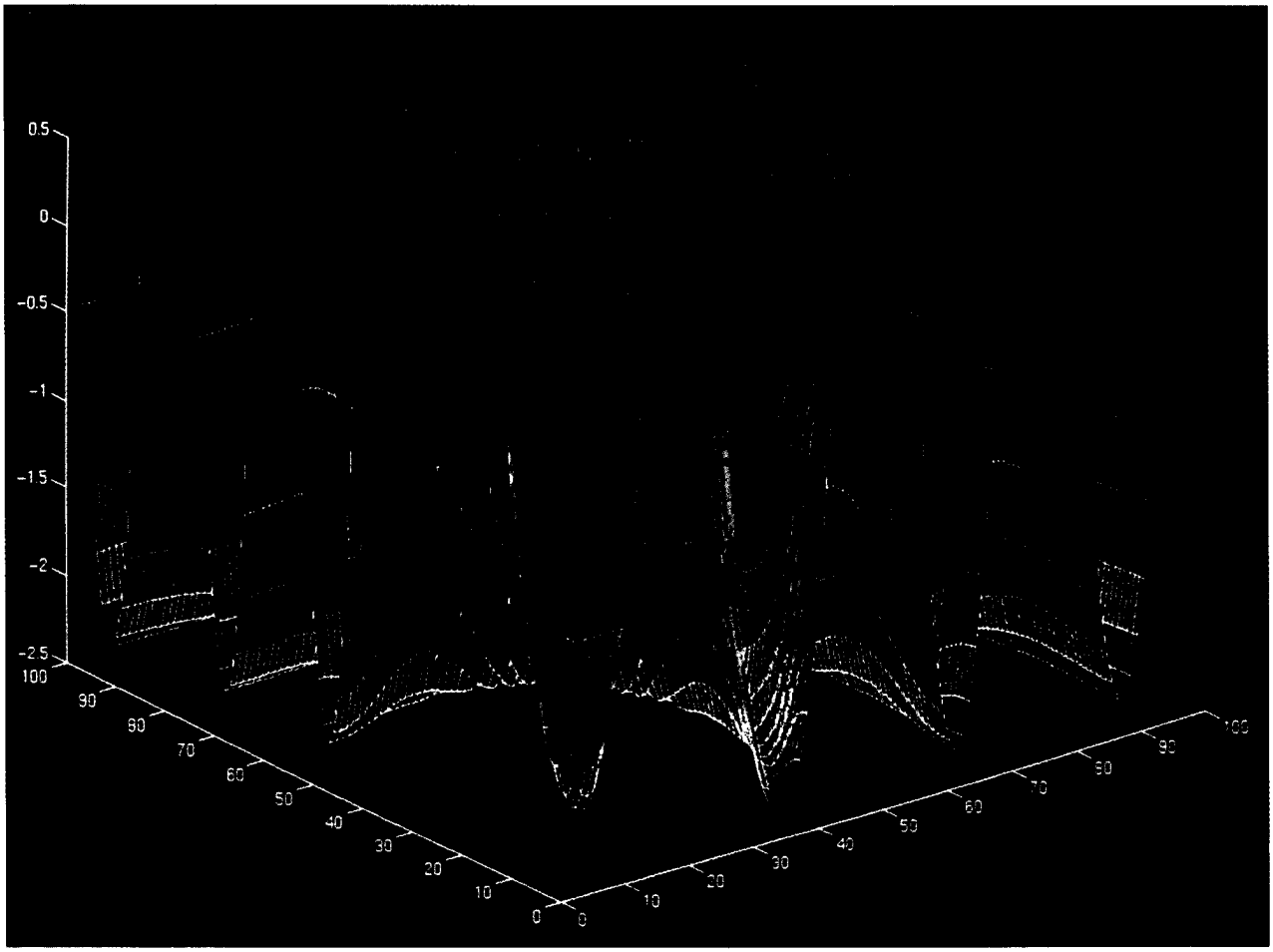

Fig. 4. A fully developed target wave in a 2-D array of 98 × 98 cells.

is initiated. The neighboring cells trigger each other through a mechanism similar to that described in Part I, Section II-A, of this tutorial. In this case, however, since each cell is monostable, it settles down to its original state after a short period of time, and the wave front disappears when it reaches the boundary of the array. A series of concentric wave fronts can be induced by forcing the center cell periodically (Fig. 1). When forced with a periodic signal of the form $A\cos(wt)$ the response of the other cells, and hence the density and frequency of the wave fronts, will depend on the amplitude A and frequency w of the forcing, as well as on D. It has been known that the response of an oscillator to such forcing can be very complicated, giving rise to the so-called devil's staircase [7]–[9]. The situation is no different in coupled arrays of oscillators as long as the diffusion coefficient is large enough, i.e., the devil's staircase structure translates into arrays without any change ((Fig. 2(a)). A more complicated response is observed if the diffusion coefficient is small, resulting in the breakdown of the devil's staircase which no longer represents a monotone increasing function [Fig. 2(b) and (c)]. Among other phenomena observed from such responses in arrays is the appearance of noninteger winding numbers (e.g., for $A = 1.2$,$\omega = 1.238$ in which case the winding number $W = 3.5$) in contrast to integer ones in single forced cells.

B. Target Waves in a Fluctuating Medium

With the parameter values

$$\alpha = 10, \quad \beta = 0.334091, \quad s_1 = 0.020706, \quad s_2 = 15, \quad s_0 = -0.921, \quad \epsilon = 0 \tag{4}$$

corresponding to a periodic regime in each cell, and initial conditions from Section III-A, Part I, a spiral wave is generated. By placing a U-shaped obstacle in the path of the spiral, which is accomplished by clamping appropriate cells ($(i, 10)$, $(i, 20)$ for $i = 10, 11, \cdots, 20$, and $(10, k)$ for $k = 10, 11, \cdots, 20$)) at fixed values (e.g., at (-1.25, 0, 1.25)), the spiral structure is gradually destroyed and a sustained train of concentric waves takes over, with the obstacle as the "source" (Figs. 3 and 4). Thus by changing the boundary condition, a different type of wave is generated.

C. Interactions of Autowaves in Excitable Media

There is a fundamental difference in the properties of autowaves and classical waves in conservative systems. During the propagation of autowaves, the shape and amplitude remain constant, in contrast to classical waves which become distorted

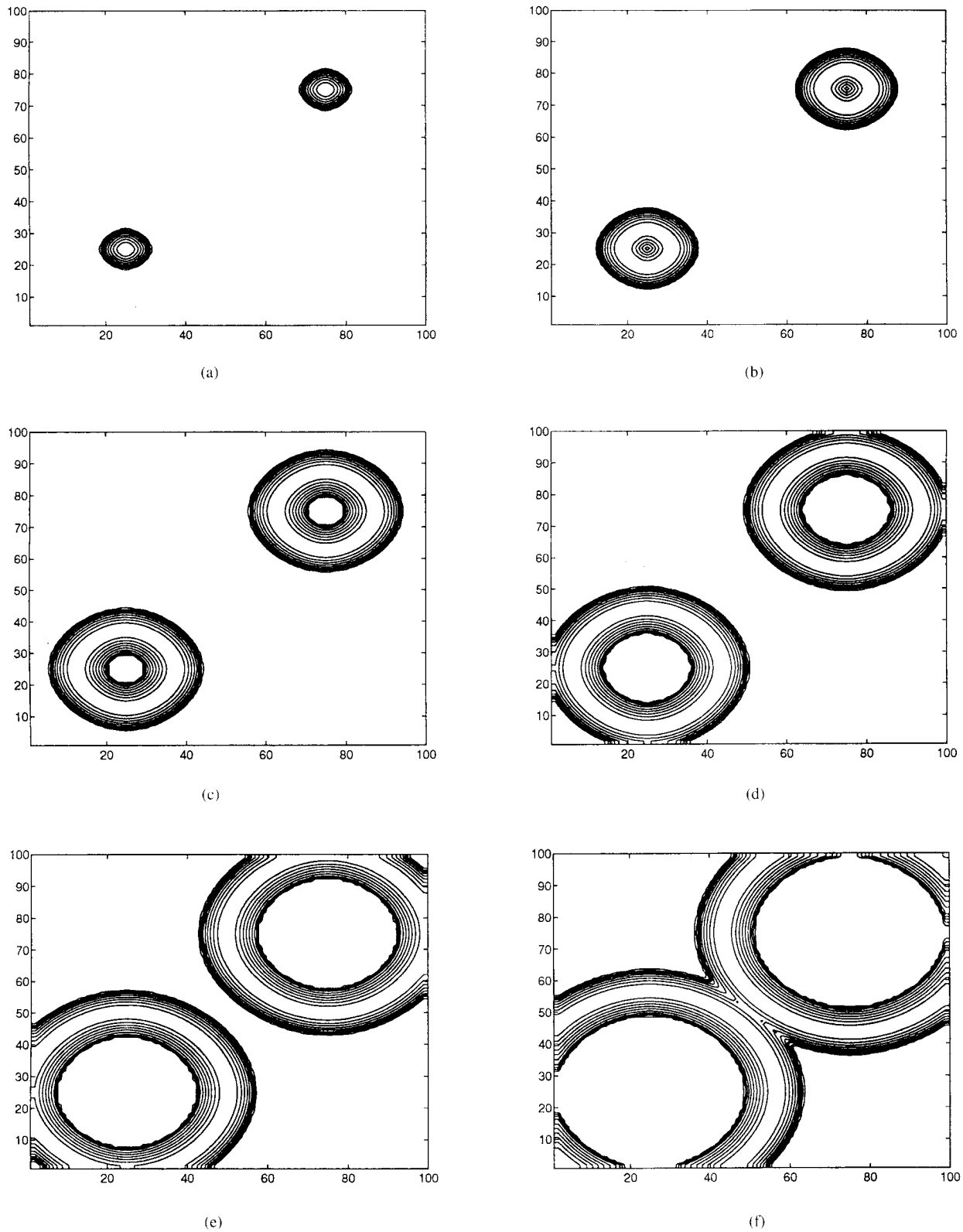

Fig. 5. Two target waves annihilate upon collision. x variables of cells (25, 25) and (75, 75) were set to -3 every 10 time units. Snapshots (a) through (j) correspond to $t = 20, 40, 60, \cdots, 200$.

through diffusion processes in the media. Autowaves do not reflect from each other upon collision, nor do they penetrate or interfere with one another, but they annihilate instead. This is clearly demonstrated in an interaction of two target waves in Fig. 5. Two cells are excited periodically to generate concentric wavefronts that annihilate when they collide. The

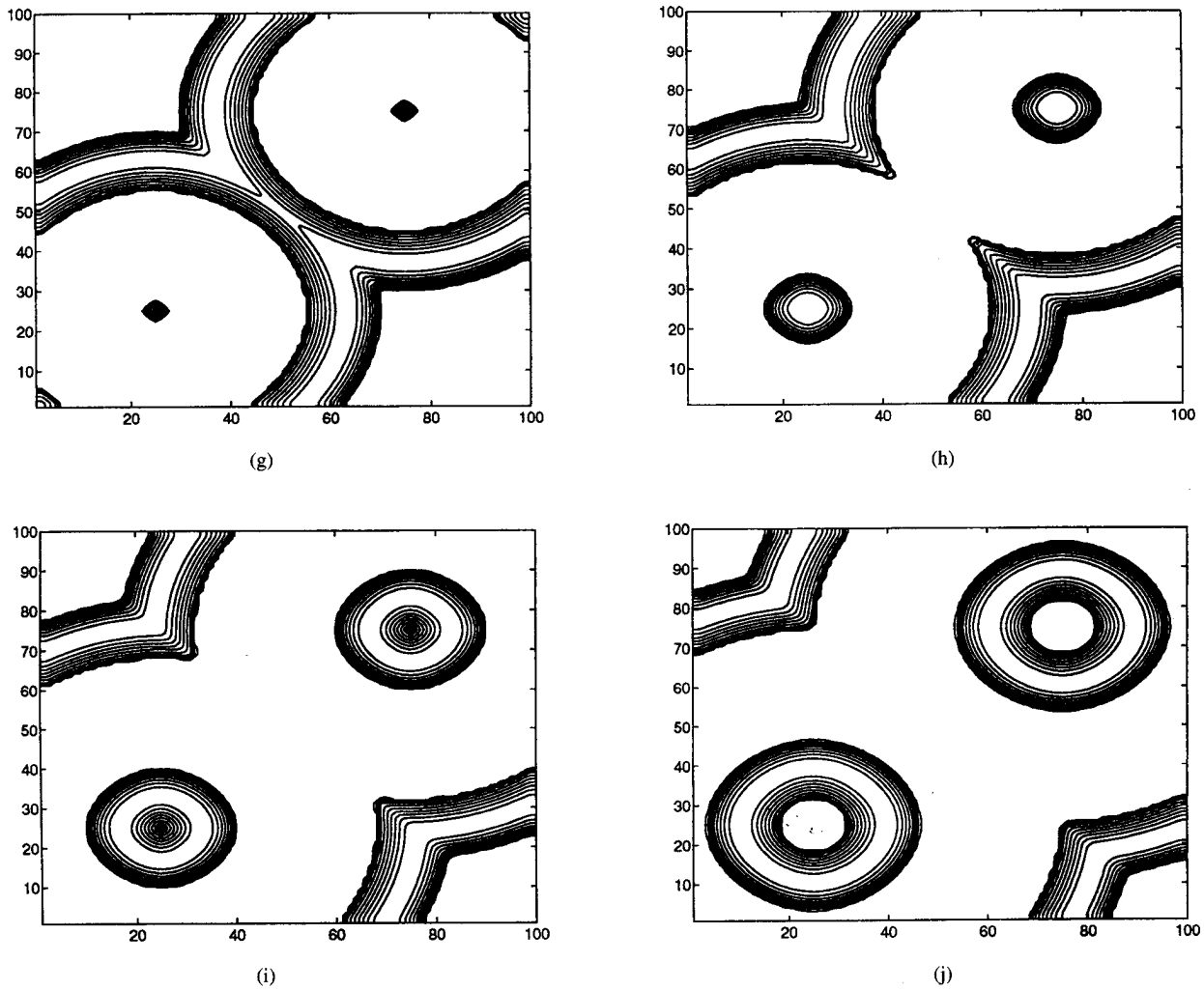

Fig. 5. *(Continued.)*

annihilation property makes it possible for multiple spirals to coexist (Fig. 6), without destroying or interfering with one another.

However, despite the annihilation property, coexistence of two types of autowaves is only temporary if one of them causes reexcitation of array cells with a higher frequency. The spiral wave in Fig. 7 propagates through the medium faster than the target wave, resulting in a gradual swamping of the concentric wave pattern.

III. Scroll Waves in 3-D CNN Arrays

We consider 3-D CNN arrays of resistively coupled Chua's circuits each of which operates in a periodic (stable limit cycle) regime. The associated dynamical system is described by the following system of equations

$$\begin{aligned}\dot{x}_{i,j,k} &= \alpha(y_{i,j,k} - x_{i,j,k} - f(x_{i,j,k})) \\ &\quad + D_{i,j,k}(x_{i+1,j,k} \\ &\quad + x_{i-1,j,k} + x_{i,j+1,k} + x_{i,j-1,k} \\ &\quad + x_{i,j,k+1} + x_{i,j,k-1} - 6x_{i,j,k}) \\ \dot{y}_{i,j,k} &= x_{i,j,k} - y_{i,j,k} + z_{i,j,k} \\ \dot{z}_{i,j,k} &= -\beta y_{i,j,k} \quad (1 \le i \le N_i, 1 \le j \le N_j, 1 \le k \le N_k)\end{aligned}$$

where

$$\begin{aligned}f(x) = (1/2)[&(s_2 + s_1)x + (s_0 - s_2)(|x - B_1| - |B_1|) \\ &+ (s_1 - s_0)(|x - B_2| - |B_2|)]\end{aligned}$$

is a 3-segment piecewise-linear function with the slopes $s_0 = -0.921$ (middle segment), $s_1 = 15$ (right-hand segment), $s_2 = 0.020206$ (left-hand segment), and the breakpoints $B_1 = -1$, $B_2 = 0.0591173$. These parameters and $\alpha = 10$, $\beta = 0.334091$, as well as diffusion coefficients $D_{i,j,k} = D = 0.1$ will be fixed unless otherwise stated. Also the size of the 3-D array was the same in all simulations, namely $N_i = N_j = N_k = 50$.[1] We used Euler's integration routine and stepsize 0.01 to integrate the system. In all cases, zero flux (Neumann) boundary conditions were used. We consider three types of scroll waves: the straight scroll wave, twisted scroll wave, and scroll ring wave.

a) *Straight scroll waves* can be generated from the initial conditions in which the "2-D" initial conditions for spiral generation (see Section III-A, Part I) are simply stacked one on top of the other in the 3-D array in one

[1] Considering zero flux boundary condition, the actual array size is 48 × 48 × 48. Similarly in other arrays.

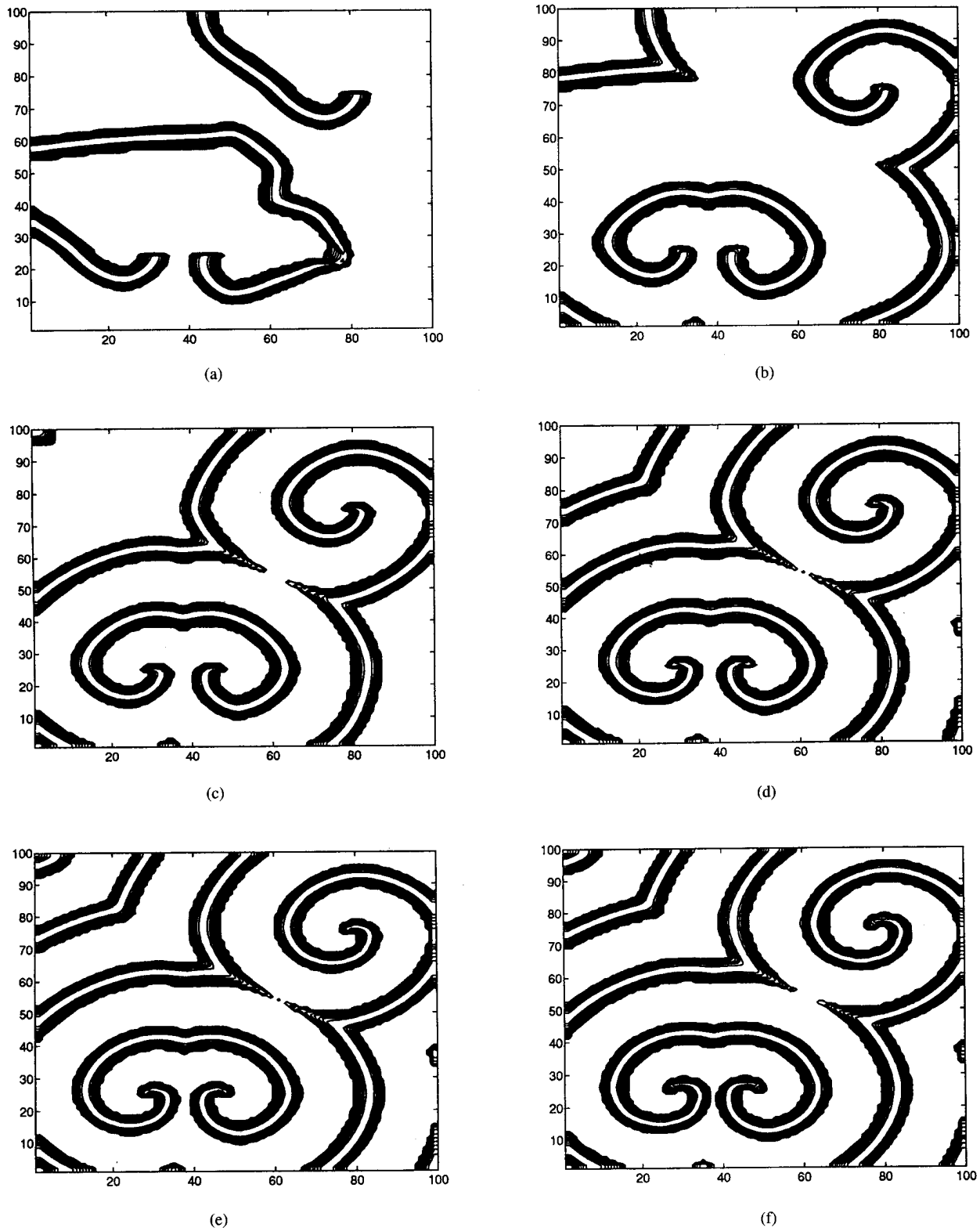

Fig. 6. Coexistence of multiple spirals in excitable medium ($D = 0.5$). Parameter values (3) and standard initial conditions for spiral generation (Section III-A, Part I) were used in the first and third quadrants of the 98 × 98 array. Other cells were set to equilibrium $\mathbf{P}^+$. Snapshots at $t = 20$, 40, 60, 80, 100, 200.

direction. Fig. 8 shows a projection of the isosurfaces of the resulting scroll wave. Note the two wavefronts corresponding to the same level of variable x for the isosurfaces.

b) *Twisted scroll waves* can be produced in two ways.

1) In homogeneous medium, the initial conditions can be generated from those for the straight scroll wave through the rotation, by appropriate angles, of in-

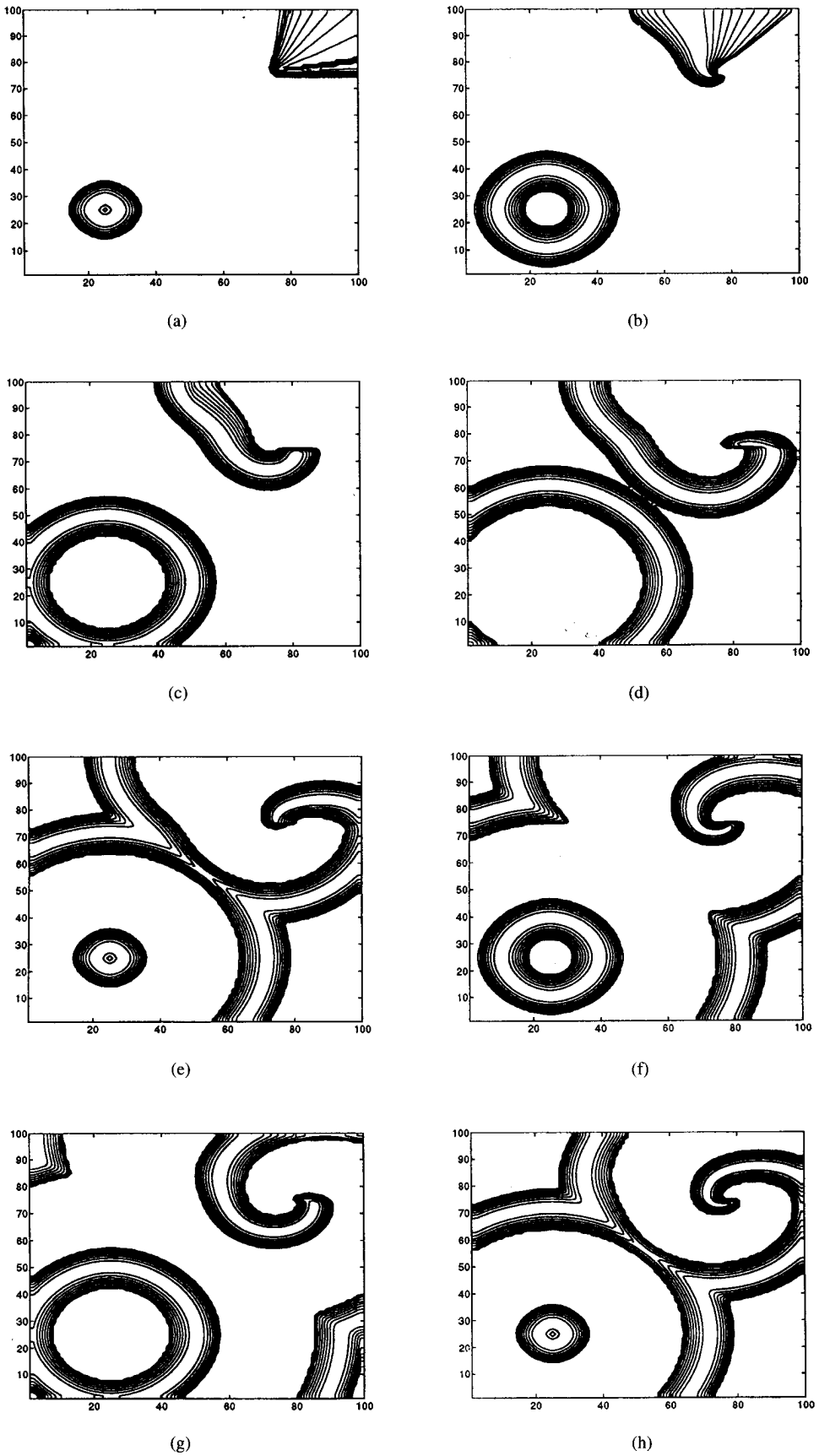

Fig. 7. Spiral and target wave interaction in excitable medium ($D = 0.5$). Initial conditions for spiral generation were used in the first quadrant of the 98 × 98 array, and the x variable of cell (25, 25) was set to -3 every 10 time units to generate the interaction. The target wave was swept away by the spiral after about 500 time units. Snapshots (a) through (p) correspond to $t = 5$, 10, 15, 20, 25, 30, 35, 50, 70, 90, 110, 130, 150, 170, 330, and 450, respectively.

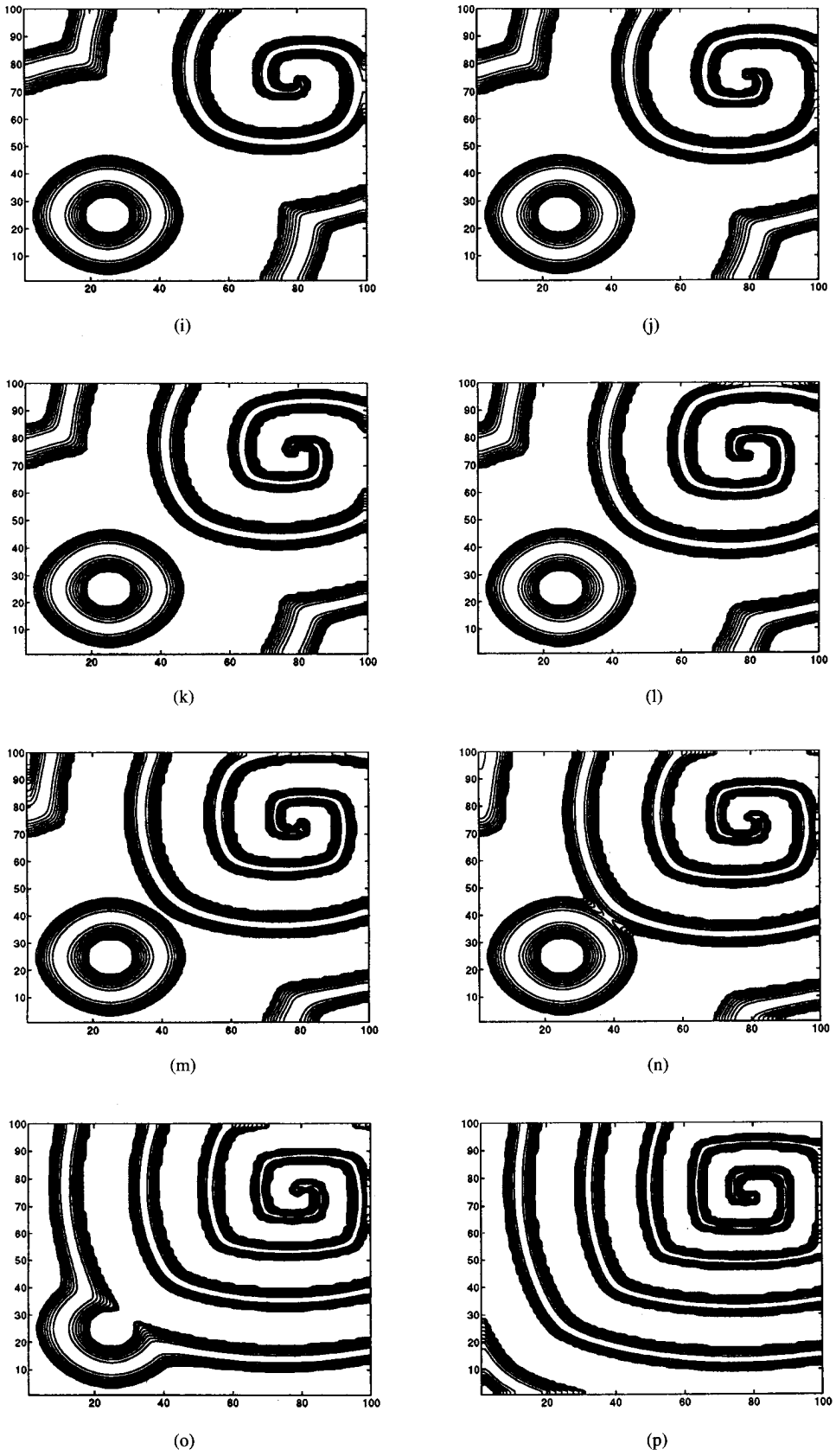

Fig. 7. *(Continued.)*

dividual 2-D layers of the 3-D array. An example of this type of twisted scroll wave is given in Fig. 9. According to [10], twisted scroll waves in homogeneous medium are unstable, and tend to untwist for large simulation times, which was indeed the case with our particular simulation.

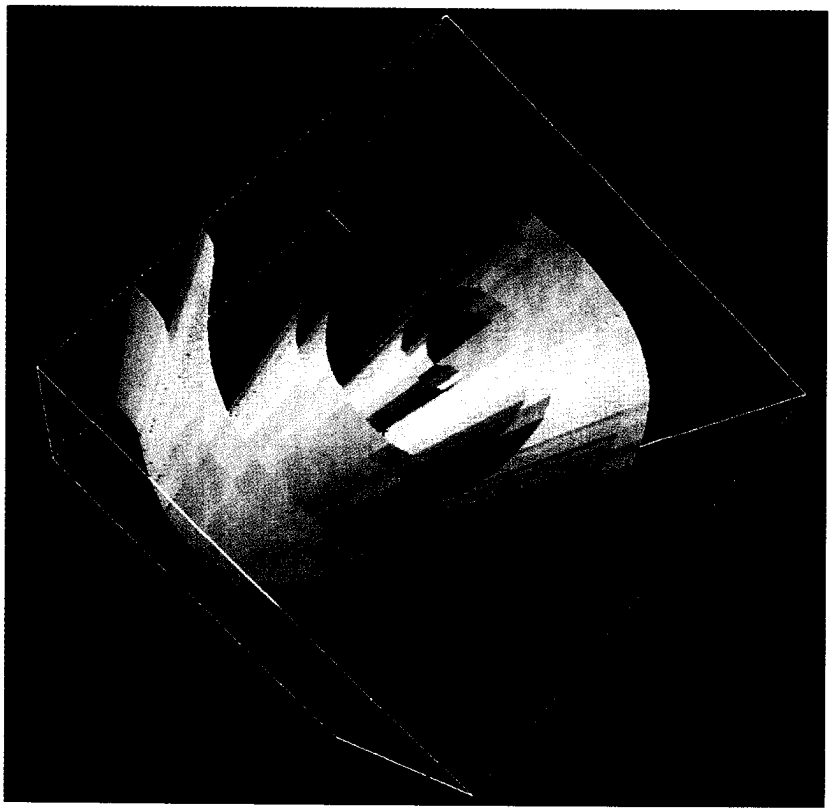

Fig. 8. Isosurfaces for a straight scroll wave, generated from a 48 × 48 × 48 array of Chua's circuits. Here, as well as in all subsequent figures, the isosurfaces correspond to the level −1.503 of variable x.

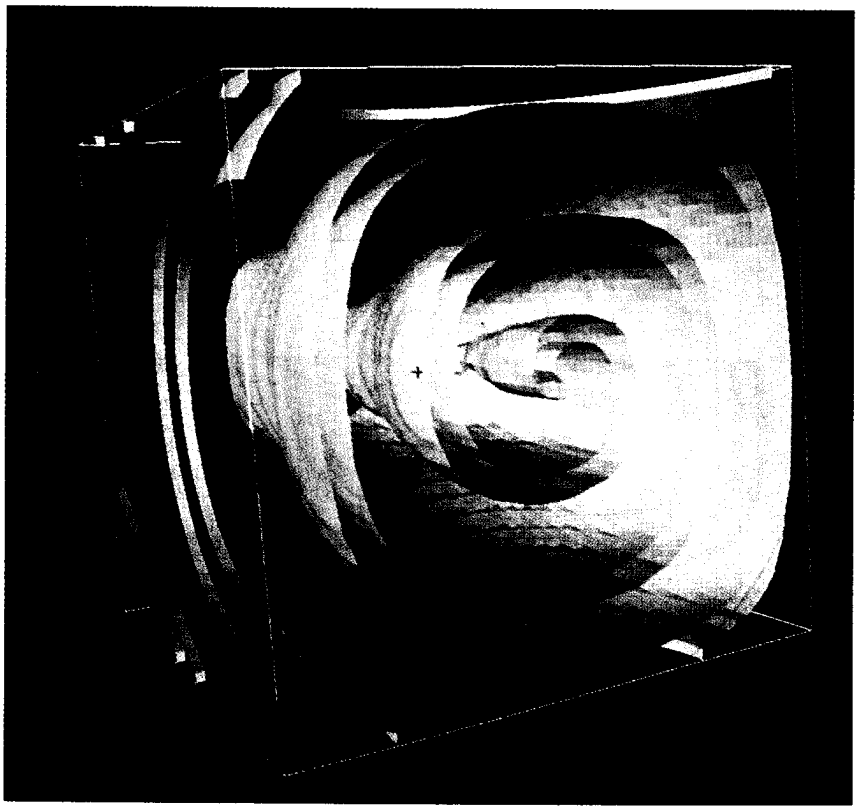

Fig. 9. Twisted scroll wave generated in a homogeneous discrete active medium, at time $t = 80$. Initial conditions were obtained through gradual rotation of a developed spiral by angle 4π from top to bottom of array. The scroll wave has untwisted by almost 3π by the time $t = 3000$.

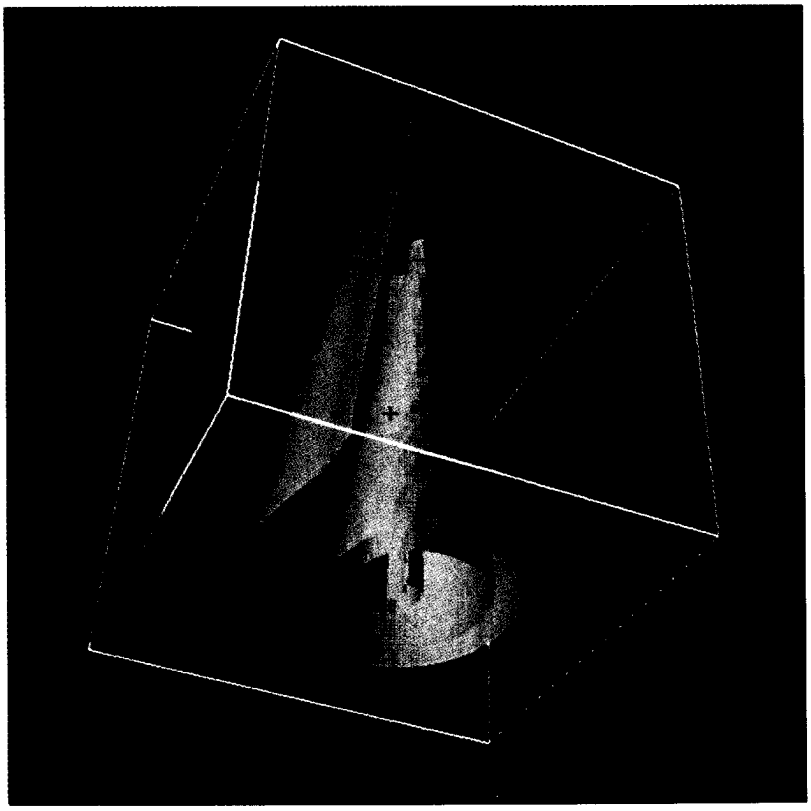

(a)

(b)

Fig. 10. (a) Inhomogeneous discrete active media give rise to twisted scroll waves. The snapshot is at time $t = 300$. (b) Snapshot of the wave at $t = 3000$.

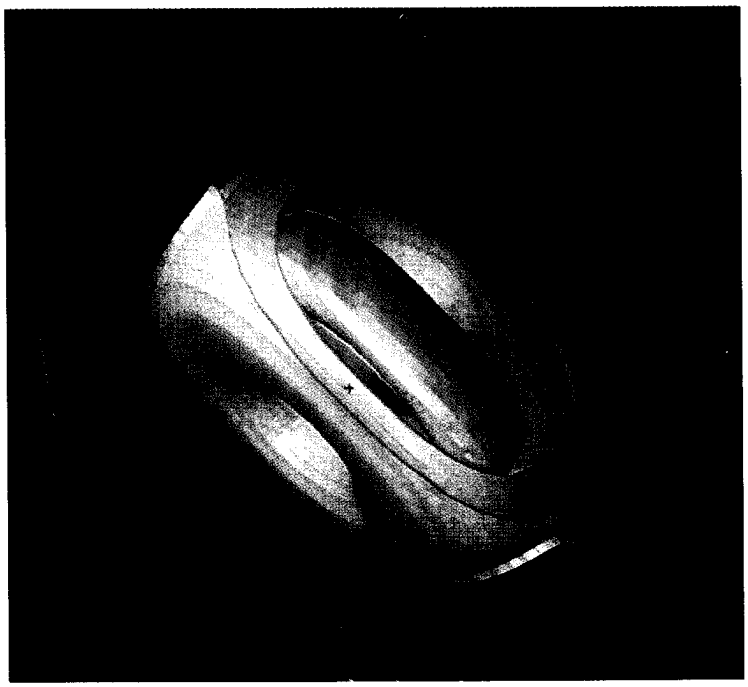

(a)

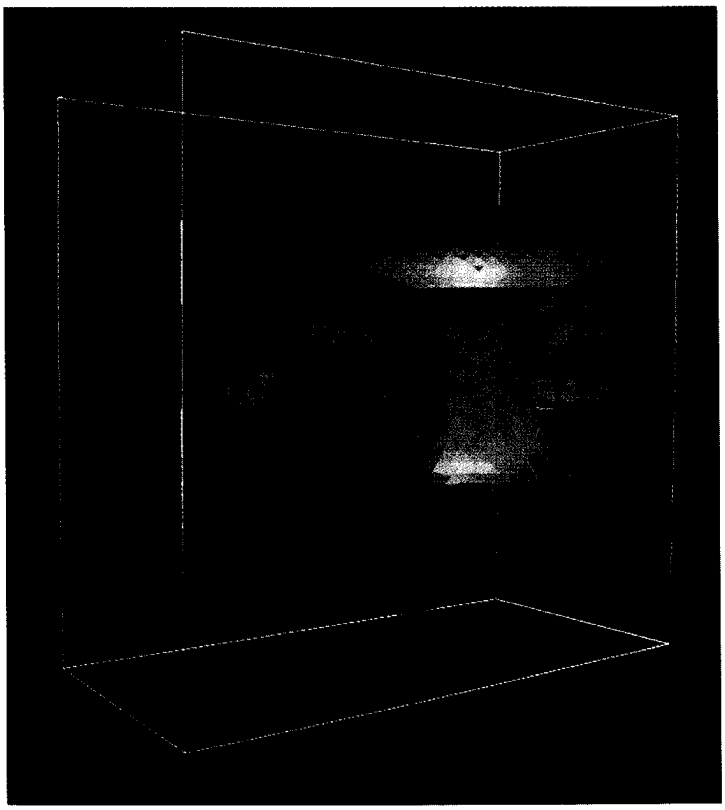

(b)

Fig. 11. (a) Scroll ring at $t = 700$. (b) Cross section of the scroll ring at level $j = 25$.

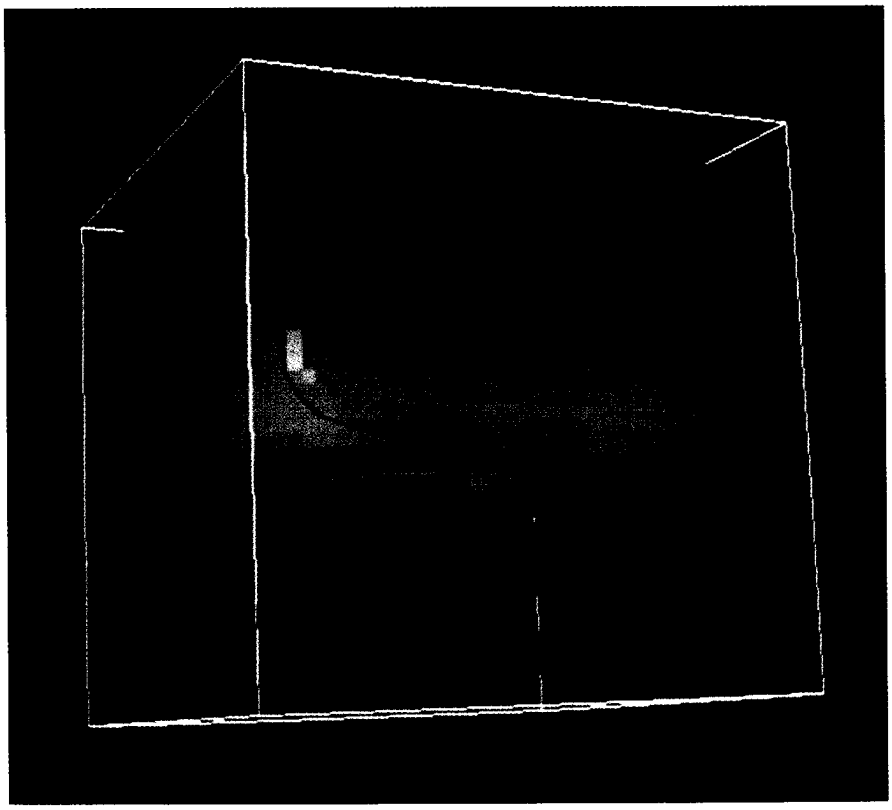

(a)

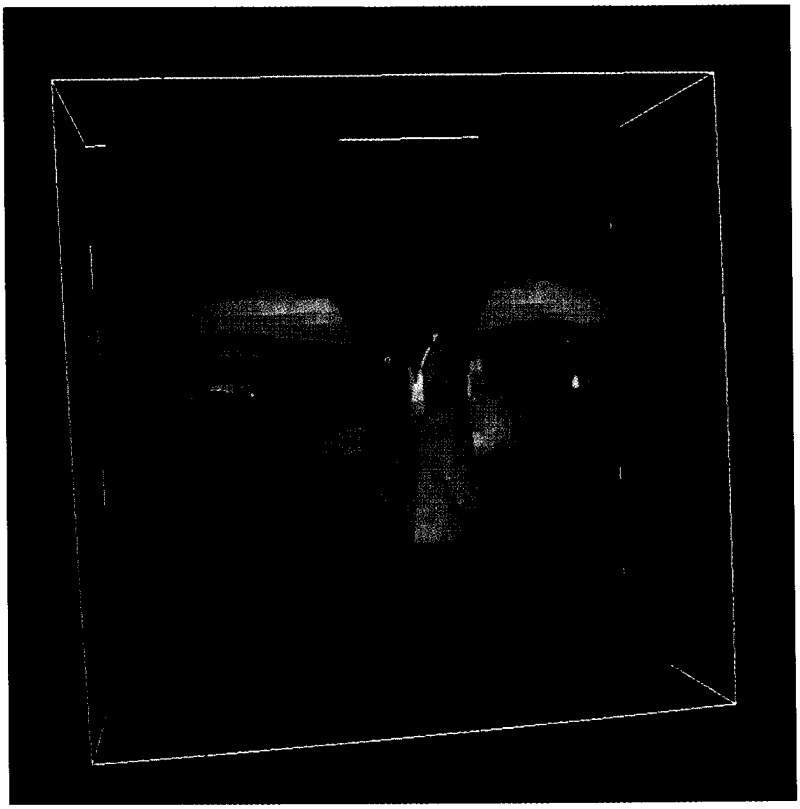

(b)

Fig. 12. (a) Scroll ring in its later stages of development at $t = 3000$. (b) Cross section of the scroll ring at level $j = 25$.

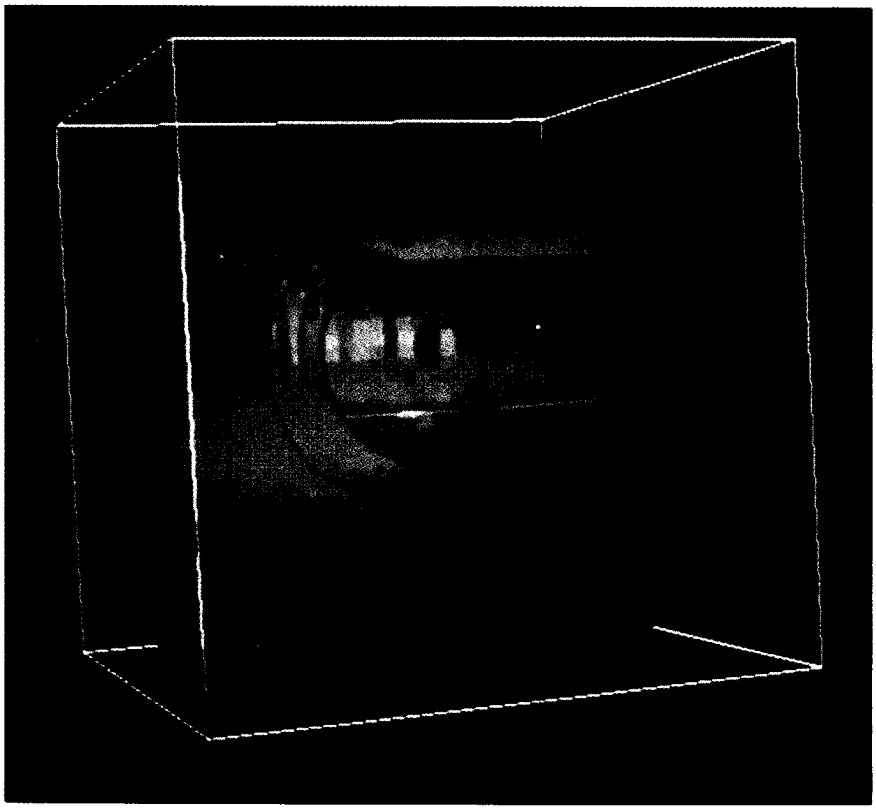

Fig. 13. Scroll ring created through the rotation of a developed spiral ($t = 0$).

2) Another way of obtaining twisted scroll waves is to use an inhomogeneous medium, e.g., by introducing a uniform gradient for the diffusion coefficient, in the k–direction for instance, as follows: $D_{i,j,k} = D(1 + k/25)$, i.e., $D_{i,j,k}$ varies between 0.1 and 0.3 (Fig. 10). Since larger diffusion coefficients give rise to greater wavelengths and smaller periods of rotation, the initial conditions evolve into a twisted scroll wave which, in contrast to 1), is stable [11]. Different shapes and degree of twist can be achieved by simultaneously imposing a gradient to parameters α and D.

c) *Scroll ring waves* have been previously studied numerically, e.g., in [12], using the classical FitzHugh–Nagumo equations. Here we use the same parameter values as in a) and b1), and change only the initial conditions. A scroll ring can be thought of as the trace of a spiral, rotated along a circle in the three-dimensional space. In our particular case we used the mapping

$$x(i,j,k) = X(i, I(N/4) + I(\sqrt{(j - N/2 - 1)^2 + (k - N/2 - 1)^2}))$$

where N is the array size ($N = 50$ in our case), $I(r)$ is the nearest integer approximation to real number r, and $X(m,n)$ is the x-variable of the cell with coordinates (m,n) in the 2-D array of initial conditions for the spiral. The same formulae were used for the y- and z-variables. A scroll ring develops after about 1000 time units. Although circular in its early stages (Fig. 11(a)), it developed "corners" after several thousand time units (Fig. 12(a)). On a larger time scale, the scroll waves were unstable, drifting along their axes and disintegrating after hitting the boundary of the medium. The objects in Figs. 11–13 seem to resemble tori at first sight, but their cross sections (Figs. 11(b) and 12(b)) reveal a scroll structure.

Finally, let us observe that the above simulations were all performed for parameter values corresponding to an active medium with periodic (limit cycle) local behavior. However, similar results can also be obtained by using excitable dynamics of the local cell behavior, e.g., by modifying the parameter values to $\beta = 0.3014987$, $D = 0.2$, $s_0 = -1.25719$, $s_2 = 0.078573$, and using the same initial conditions as above.

IV. Spatio-Temporal Chaos in Rings of Chua's Circuits

One-dimensional CNNs consisting of resistively coupled Chua's circuits can exhibit a variety of spatio-temporal phenomena which are typical of spatially extended reaction-diffusion media.

An investigation of spatio-temporal dynamics was conducted in [13] for the system governed by equations

$$\begin{aligned} \dot{x}_k &= \alpha(y_k - f(x_k)) + D(x_{k-1} - 2x_k + x_{k+1}) \\ \dot{y}_k &= x_k - y_k + z_k \quad (k = 1, \cdots, l) \\ \dot{z}_k &= -\beta y_k \end{aligned} \tag{5}$$

where

$$f(x) = (1/2)[(s_1 + s_2)x + (s_0 - s_1)(|x - B_1| - |B_1|) + (s_2 - s_0)(|x - B_2| - |B_2|)] \tag{6}$$

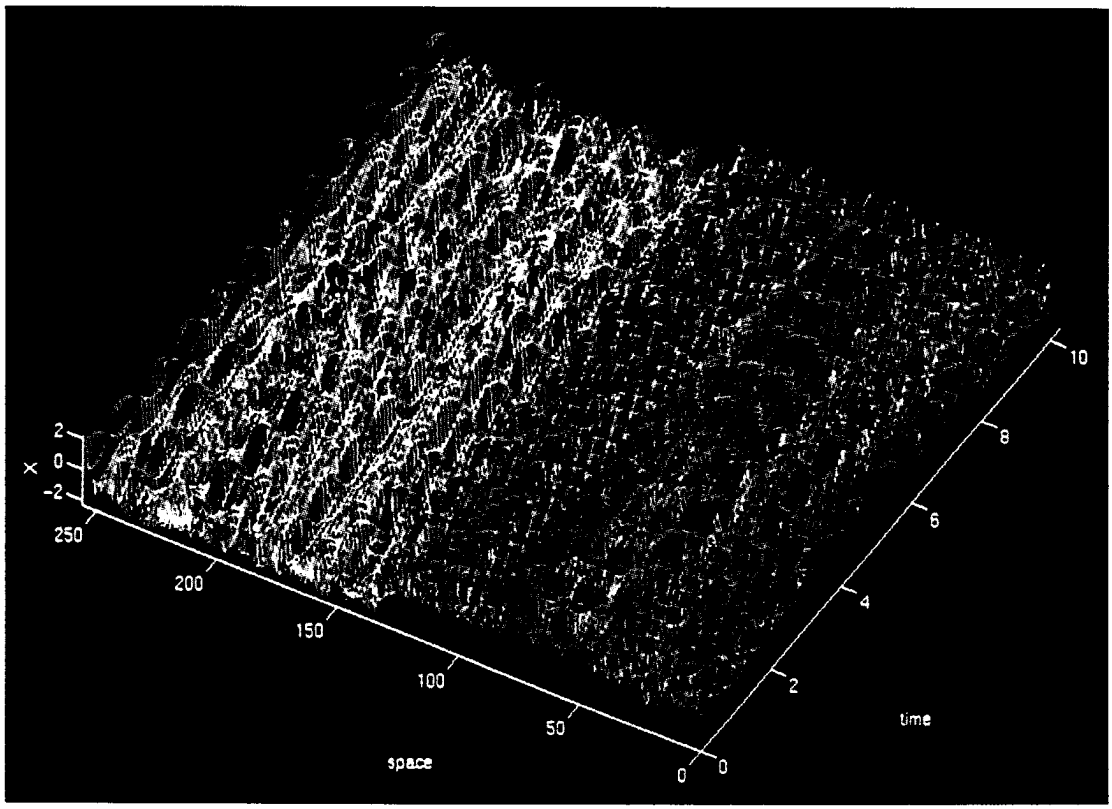

Fig. 14. Chaotic spatio-temporal pattern of the variable x for initial conditions (7) and diffusion coefficient $D = 0.4$, in a ring of $N = 256$ cells.

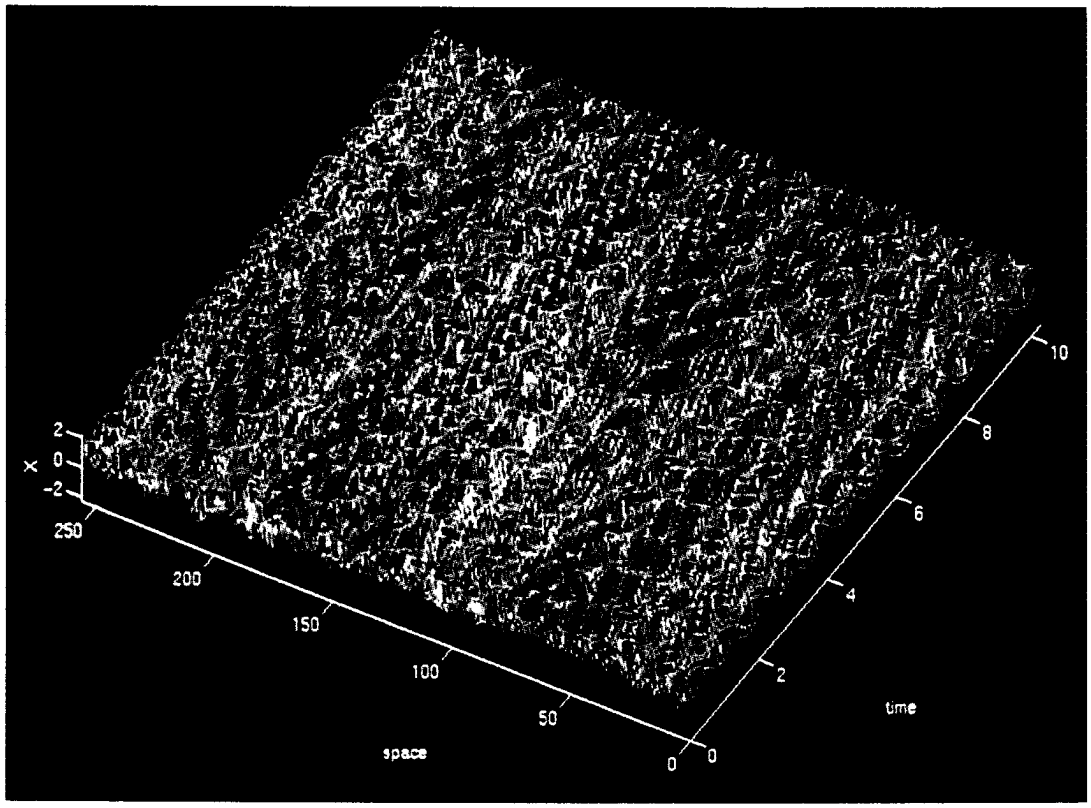

Fig. 15. Result corresponding to Fig. 14 for initial conditions (8).

is a three-segment piecewise-linear function with breakpoints $B_1 = -1$ and $B_2 = 1$; α and β are appropriately scaled circuit parameters, and $D = \alpha/(GR)$ is the diffusion coefficient. We can choose parameter values $\alpha = 9$, $\beta = 19$, slopes $s_1 = -5/7$,

$s_0 = -8/7$, $s_2 = -5/7$, and periodic boundary conditions $x_0 = x_N$, $x_{N+1} = x_1$, where N is the number of cells in the ring; similarly for y and z variables.

The parameters for an uncoupled Chua's circuit were chosen so that it has two stable limit cycles, symmetrical with respect to origin. Despite simple local dynamics of the basic cell, the global behavior of the system can be very complicated. The dynamics were studied for two types of initial conditions. In the first type

$$x_j(0) = 1 + 0.1 \sin \frac{2\pi(j-1)}{N}, \quad y_j(0) = z_j(0) = 0 \quad (7)$$

the trajectories of all cells are attracted to the same limit cycle. In the second type

$$x_j(0) = \sin \frac{2\pi(j-1)}{N}, \quad y_j(0) = z_j(0) = 0.1 \quad (8)$$

the trajectories of cells belong to the basins of attraction of two different limit cycles. The computations showed that for both types of initial conditions, the dynamics of the system have much in common. For weak couplings ($D \ll 1$), the spatio-temporal patterns in both cases are simple: weakly inhomogeneous in space and periodic in time. When the diffusion coefficient D exceeds the critical value D_{cr}, a pattern occurs—so called π-spatial oscillation—where almost all adjacent cells are 180° out of phase. Increasing the diffusion coefficient D further gives rise to envelope waves against a background of π-oscillations and finally, when $D \geq 0.33$, chaotic spatio-temporal patterns appear. We can see that these patterns no longer exhibit any regular structures in space and are chaotic (with broadband power spectrum) in time. Chaotic spatio-temporal patterns were further studied based on a new approach describing the properties of patterns through characteristics of associated attractors of a multidimensional dynamical system with *matrix* phase space. Using this approach it has been found that the attractors corresponding to the chaotic patterns for initial conditions (7) (Fig. 14) have large correlation dimension (>10), whereas for initial conditions (8) (Fig. 15) the correlation dimension is low (<5). Thus, it is shown that in the matrix phase space of CNNs, different high- and low-dimensional attractors coexist, corresponding to different initial conditions.

The investigations show that the spatio-temporal dynamics of 1-D CNNs are extremely rich and require detailed and systematic analysis. Such investigation can elucidate the spatio-temporal phenomena occuring not only in CNNs but in a broad range of spatially extended reaction-diffusion media as well.

ACKNOWLEDGMENT

The computations were partly performed on the Cray C90 supercomputer at the CEWES HPC Center, Vicksburg, MS.

REFERENCES

[1] A. T. Winfree, "Scroll-shaped waves of chemical activity in three dimensions," *Science*, vol. 181, pp. 937–939, 1973.
[2] R. N. Madan, Ed., *Chua's Circuit: A Paradigm for Chaos*. Singapore: World Scientific, 1993.
[3] T. Amemori, N. A. Gorelova, and J. Bures, "Spreading depression in the olfactory bulb of rats: reliable initiation and boundaries of propagation," *Neuroscience*, vol. 22, pp. 29–36, 1987.
[4] P. S. Chen, P. D. Wolf, E. G. Dixon, N. D. Danieley, D. W. Frazier, W. M. Smith, and R. E. Ideker "Mechanism of ventricular vulnerability to single premature stimuli in open chest dogs," *Circulation Res.*, vol. 62, pp. 1191–1209, 1988.
[5] A. M. Pertsov, E. A. Ermakova, and A. V. Panfilov "Rotating spiral waves in a modified Fitzhugh–Nagumo model," *Physica*, vol. 14D, pp. 117–124, 1984.
[6] W. Jahnke and A. T. Winfree "A survey of spiral-wave behaviors in the Oregonator model," *Int. J. Bifurc. and Chaos*, vol. 1, no. 2, pp. 445-466, 1991.
[7] M. Itoh, H. Murakami, and L. O. Chua, "Experimental study of forced Chua's oscillator," *Int. J. Bifurc. and Chaos*, vol. 4, no. 6, pp. 1721–1742, 1994.
[8] V. Pérez-Muñuzuri, M. Alonso, L. O. Chua, and V. Pérez-Villar, "Resonance patterns in one-dimensional arrays of coupled nonlinear excitable systems," *Int. J. Bifurc. and Chaos*, vol. 4, no. 6, pp. 1631–1638, 1994.
[9] L. Pivka, A. L. Zheleznyak, and L. O. Chua, "Arnol'd tongues, devil's staircase, and self-similarity in the driven Chua's circuit," *Int. J. Bifurc. and Chaos* vol. 4, no. 6, pp. 1743–1753, 1994.
[10] A. S. Mikhailov, *Foundations of Synergetics I. Distributed Active Systems*. Berlin: Springer-Verlag, 1990.
[11] A. V. Panfilov, A. N. Rudenko, and A. M. Pertsov, "Twisted scroll waves in three-dimensional active media," in *Self-Organization: Autowaves and Structures Far from Equilibrium*, V. I. Krinsky, Ed. Berlin: Springer-Verlag, 1984.
[12] M. Courtemanche, W. Skaggs and A. T. Winfree "Stable three-dimensional action potential in the FitzHugh–Nagumo model," *Physica*, vol. 41D, pp. 173–182, 1990.
[13] A. L. Zheleznyak and L. O. Chua, "Coexistence of low- and high-dimensional spatio-temporal chaos in a chain of dissipatively coupled Chua's circuits," *Int. J. Bifurc. and Chaos*, vol. 4, no. 3, pp. 639–674, 1994.

Ladislav Pivka, for a photograph and biography, see this issue, p. 637.